KLHL40 deficiency destabilizes thin filament proteins and promotes nemaline myopathy

Ankit Garg,[1] Jason O'Rourke,[1] Chengzu Long,[1] Jonathan Doering,[2] Gianina Ravenscroft,[3] Svetlana Bezprozvannaya,[1] Benjamin R. Nelson,[1] Nadine Beetz,[1] Lin Li,[4] She Chen,[4] Nigel G. Laing,[3] Robert W. Grange,[2] Rhonda Bassel-Duby,[1] and Eric N. Olson[1]

[1]Department of Molecular Biology, University of Texas Southwestern Medical Center, Dallas, Texas, USA. [2]Department of Human Nutrition, Foods, and Exercise and Metabolic Phenotyping Core, Virginia Tech University, Blacksburg, Virginia, USA. [3]Harry Perkins Institute of Medical Research, University of Western Australia, Nedlands, Western Australia, Australia. [4]National Institute of Biological Sciences, Beijing, China.

Nemaline myopathy (NM) is a congenital myopathy that can result in lethal muscle dysfunction and is thought to be a disease of the sarcomere thin filament. Recently, several proteins of unknown function have been implicated in NM, but the mechanistic basis of their contribution to disease remains unresolved. Here, we demonstrated that loss of a muscle-specific protein, kelch-like family member 40 (KLHL40), results in a nemaline-like myopathy in mice that closely phenocopies muscle abnormalities observed in *KLHL40*-deficient patients. We determined that KLHL40 localizes to the sarcomere I band and A band and binds to nebulin (NEB), a protein frequently implicated in NM, as well as a putative thin filament protein, leiomodin 3 (LMOD3). KLHL40 belongs to the BTB-BACK-kelch (BBK) family of proteins, some of which have been shown to promote degradation of their substrates. In contrast, we found that KLHL40 promotes stability of NEB and LMOD3 and blocks LMOD3 ubiquitination. Accordingly, NEB and LMOD3 were reduced in skeletal muscle of both *Klhl40*$^{-/-}$ mice and *KLHL40*-deficient patients. Loss of sarcomere thin filament proteins is a frequent cause of NM; therefore, our data that KLHL40 stabilizes NEB and LMOD3 provide a potential basis for the development of NM in KLHL40-deficient patients.

Introduction

Nemaline myopathies (NMs) encompass a set of genetically heterogeneous diseases that are defined pathologically by the presence of characteristic rod-like structures, called nemaline bodies, in myofibers (1). Clinically, presentation of NM can vary substantially from mild muscle dysfunction to complete akinesia, but without any correlation to the number of nemaline bodies, suggesting that these structures are not a primary cause of the muscle dysfunction (2). The underlying pathogenesis of NM remains unresolved; however, 6 of 9 causative genes for NM, tropomyosin 3 (*TPM3*), nebulin (*NEB*), α 1 actin (*ACTA1*), tropomyosin 2 (*TPM2*), troponin T type 1 (*TNNT1*), and cofilin 2 (*CFL2*), encode components of the sarcomere thin filament, leading to the current hypothesis that NM is a thin filament disease (3–8).

The sarcomere thin filament is a helical strand of polymerized actin that anchors directly to the Z line and spans toward the M line (9). During muscle contraction, thick filament myosin forms crossbridges with thin filament actin and physically pulls the Z line toward the M line to generate force. Tropomyosin and the troponin complex regulate myosin-actin crossbridges in a calcium-dependent manner. In NM, it is believed that mutations disrupting thin filament proteins result in reduced force generation and subsequent myopathy (10). However, mutations in 3 proteins with no established association with the sarcomere thin filament, kelch repeat and BTB (POZ) domain containing 13 (KBTBD13), kelch-like family member 40 (KLHL40), and KLHL41, have been shown recently to cause NM in patients by an unknown mechanism (11–13). Notably, *KLHL40* mutations occur frequently in severe forms of autosomal recessive NM (12).

KBTBD13, KLHL40, and KLHL41 belong to the BTB-BACK-kelch (BBK) protein family, named for the presence of BTB, BACK, and kelch repeat (KR) domains in all family members (KBTBD13 lacks an annotated BACK domain but is still very closely related to other BBK family members) (14). BBK proteins are thought to serve as substrate-specific adaptors for the cullin 3 (CUL3) E3 ligase complex, mediating the ubiquitination and, in most cases, degradation of their respective substrates (15–22). Because NM is so tightly associated with thin filament proteins, it is likely that these 3 BBK proteins also regulate the thin filament in some manner, though this has not been demonstrated. Additionally, since other BBK proteins act through the ubiquitin-proteasome system, defining the function of these proteins may facilitate therapeutic manipulation, given the availability of proteasome inhibitors for patient use.

While searching for new potential regulators of muscle function, we uncovered a novel muscle-specific transcript, *Klhl40*, that encodes for a protein localizing to the sarcomere I band and A band. Deletion of the *Klhl40* locus in mice results in sarcomere defects, with subsequent muscle dysfunction and early postnatal lethality, which closely phenocopy the muscle abnormalities observed in humans with *KLHL40* mutations (12). We show that KLHL40 binds to NEB, a thin filament protein frequently associated with NM (1), as well as leiomodin 3 (LMOD3), a novel muscle

Conflict of interest: The authors have declared that no conflict of interest exists.
Submitted: January 2, 2014; **Accepted:** May 13, 2014.
Reference information: *J Clin Invest*. 2014;124(8):3529–3539. doi:10.1172/JCI74994.

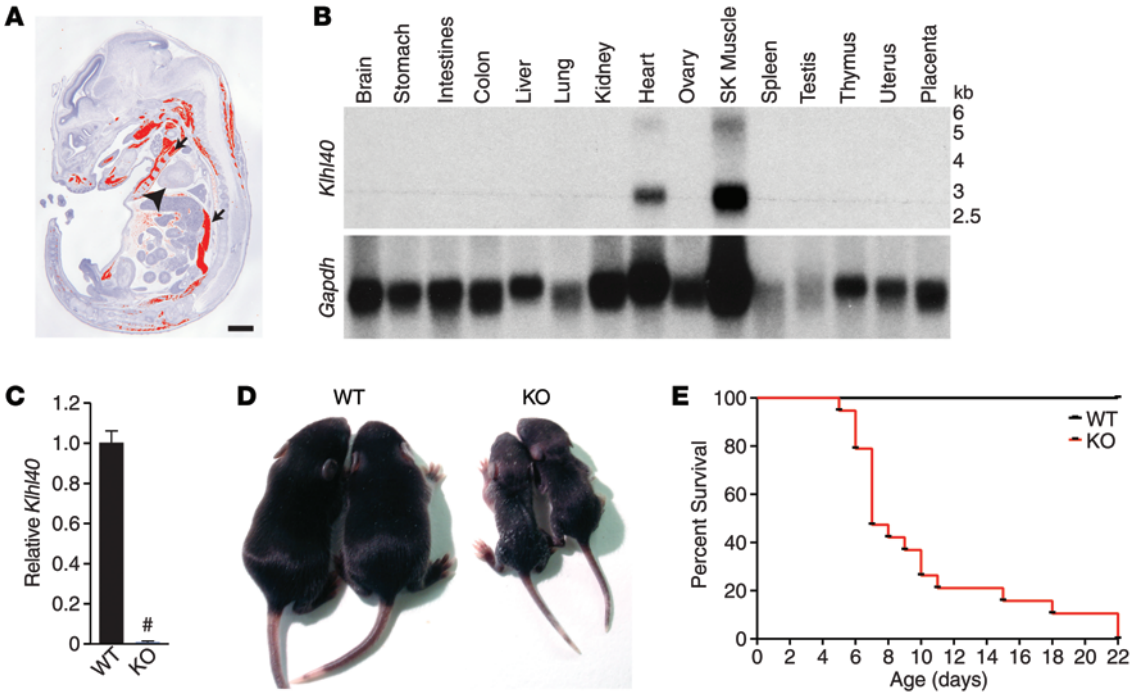

Figure 1. *Klhl40* is expressed specifically in skeletal muscle and heart, and deletion of *Klhl40* causes neonatal lethality. (**A**) Sagittal sections of E15 mouse embryos were probed for *Klhl40* mRNA using antisense radioisotopic probes. Signal for *Klhl40* (pseudocolored red) only appears in developing muscle. Black arrows point to representative developing intercostal and back muscles from rostral to caudal, respectively. The black arrowhead denotes heart. Scale bar: 1 mm. (**B**) Northern blot of adult mouse tissues for *Klhl40* and *Gapdh* (loading control) shows *Klhl40* expression in skeletal muscle and heart. Numbers on right indicate size of transcripts in kilobases. SK Muscle, skeletal muscle. (**C**) qPCR analysis of *Klhl40* transcript in P8 quadriceps in mice of the indicated genotypes. Values are normalized to 18S ribosomal RNA ($n = 3$ for both genotypes). $^{\#}P < 0.05$. (**D**) Representative image of surviving P8 KO pups with WT littermates. (**E**) Survival curve of WT versus KO mice shows early neonatal lethality in KO mice (WT, $n = 21$, and KO, $n = 17$).

protein highly homologous to leiomodin 2 (LMOD2), which regulates actin at the thin filaments (23, 24). Similar to LMOD2, we found that LMOD3 also localizes to the sarcomere thin filaments. Unlike most other BBK proteins that mediate degradation of their substrates, KLHL40 uniquely promotes stability of NEB and LMOD3 and inhibits ubiquitination of LMOD3. Accordingly, loss of KLHL40 reduces NEB and LMOD3 protein in mice as well as in patients with NM. By establishing a novel pro-stability function of KLHL40 for the thin filament proteins NEB and LMOD3, our data reveal a molecular basis for NM in patients deficient for KLHL40 and suggest a previously unrecognized role of LMOD3 in maintenance of sarcomere function and NM.

Results

Discovery and analysis of striated muscle-specific expression of Klhl40. To find new regulators of striated muscle biology, we searched an in situ hybridization database for novel transcripts that were enriched in developing muscle structures (25). Within this database, we saw that *Klhl40* appeared to have muscle-specific expression, which we found was dependent on the MEF2 transcription factor (26). We validated this muscle-specific expression in embryos and found it preserved into adulthood, with additional low level expression of *Klhl40* in the heart (Figure 1, A and B).

To assess the potential role of *Klhl40* in muscle function, we generated a loss-of-function *Klhl40* allele by replacing the protein coding region of *Klhl40* with a *lacZ* expression cassette controlled by the endogenous *Klhl40* promoter (ref. 27 and Supplemental Figure 1; supplemental material available online with this article; doi:10.1172/JCI74994DS1). We verified, by lacZ staining in $Klhl40^{+/-}$ mice, that *Klhl40* was expressed exclusively in skeletal muscle in embryonic, neonatal, and adult mice (Supplemental Figure 2, A–C). Histological analysis revealed that lacZ was only expressed in myofibers and not connective tissues (Supplemental Figure 2D). $Klhl40^{+/-}$ hearts showed punctate lacZ staining consistent with lower *Klhl40* heart expression (Supplemental Figure 3).

Loss of Klhl40 results in neonatal lethality. $Klhl40^{-/-}$ (KO) mice had no detectable *Klhl40* transcript and were smaller than WT littermates, which was apparent within several days of birth (Figure 1, C and D, and Supplemental Figure 4). Furthermore, 50% of the KO mice died by 7 days of age, and none of these KO mice bred on a pure C57BL/6 background survived past 3 weeks of age (Figure 1E). Impaired growth was not due to competition by healthier littermates, since KO mice alone with a nursing mother also failed to survive.

To confirm that the lethal phenotype was due to loss of *Klhl40* in muscle, we generated transgenic mice expressing *Klhl40* under the control of the muscle-specific, muscle creatine kinase (*MCK*) promoter and bred the allele into the KO background (28, 29). WT and KO mice with the *MCK-Klhl40* transgene are referred to as "WT Tg" and "KO Tg," respectively. We confirmed overexpression of *Klhl40* in skeletal muscle of both WT Tg and KO Tg mice (Supplemental Figure 5A). The *MCK-Klhl40* transgene was sufficient to completely rescue the KO phenotype, such that KO Tg mice were indistinguishable

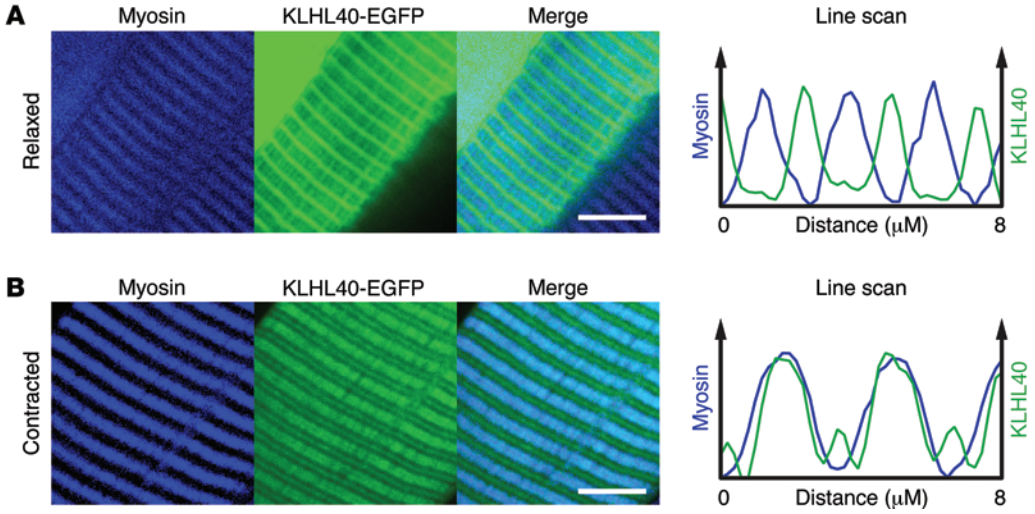

Figure 2. KLHL40 localizes to sarcomere I band and A band. KLHL40-EGFP localization relative to myosin in (**A**) relaxed muscles and (**B**) contracted muscles shows that KLHL40 localizes to the I band and A band. Graphs are representative line scans of indicated signals calculated over 8 μm of distance along the length of the myofiber. Scale bar: 5 μm.

from control littermates, with normal growth into adulthood (Supplemental Figure 5, B and C), confirming that loss of *Klhl40* from striated muscle was responsible for the neonatal lethal phenotype.

Klhl40 localizes to the sarcomere I band and A band. To better understand how loss of KLHL40 from muscle causes lethality, we analyzed the subcellular localization of KLHL40 in mature myofibers. Two previous reports on the localization of KLHL40 reported conflicting data, with one study showing A band localization of KLHL40 while another showed localization to the I band using a commercial antibody on fixed tissue sections (12, 13). To determine KLHL40 localization by an alternative method, we electroporated the flexor digitorum brevis of adult mice with KLHL40 C-terminally fused with EGFP (KLHL40-EGFP). We used second harmonic generation, as previously described, to localize KLHL40-EGFP relative to myosin (30). In a modified EDTA-Ringer's solution that relaxes myofibers (31), KLHL40-EGFP signal concentrated at the I band (Figure 2A). However, muscle bathed in a rigor solution that induces a sustained muscle contraction showed localization of KLHL40-EGFP to the A band, with fainter localization to the I band (Figure 2B and ref. 31). α-Actinin (ACTN1A) and tropomodulin (TMOD4), which are known I band and A band proteins, respectively, did not change localization in relaxed and contracted muscles (Supplemental Figure 6, A–D, and ref. 32). These data suggested that KLHL40 can localize to either the sarcomere I band or A band and indicated to us a possible role for KLHL40 in the sarcomere.

Klhl40-deficient skeletal muscle has abnormal structure and function. To determine whether loss of KLHL40 had any affect on sarcomere structure and function, we performed histologic analysis of skeletal muscles from 1-week-old neonatal KO mice and found that sarcomeres were present, but a subset of fibers showed complete disorganization, with widened Z-discs that resembled nemaline bodies present in NM (Figure 3, A and B, and ref. 1). Additionally, other myofibers in KO muscles had irregular, wave-like structures, referred to as Z line streaming (Supplemental Figure 7A). Notably, KO muscle was relatively comparable to WT muscle at 1 day of age (Supplemental Figure 7B).

To test muscle function, we measured the maximum force generated during tetanic contraction of whole hind limbs isolated from P1 mice (Figure 3C). Despite the lack of observable defects by electron microscopy analysis, P1 KO muscle demonstrated >50% reduction in hind limb strength. Consistent with the observed sarcomere dysfunction, microarray analysis of P0 quadriceps showed increased expression of sarcomere genes, possibly as a compensatory response to the underlying sarcomere defect (Supplemental Table 1). Unlike that in skeletal muscle, no differences were seen in KO heart histology or function compared with WT hearts (Supplemental Figure 8, A–C). These data suggest that KO mice have severe skeletal muscle dysfunction that likely contributes to the observed lethality.

KLHL40 binds and increases NEB and LMOD3 proteins. Because the abnormalities resulting from *Klhl40* deletion in mice resembled those found in human NM, which is thought to be a primary disease of the thin filament, we asked whether KLHL40 bound and regulated any thin filament proteins. We performed a yeast 2-hybrid screen of a human skeletal muscle cDNA prey library using KLHL40 as bait (Table 1). In parallel, we performed tandem affinity purification (TAP) of tagged KLHL40 from C2C12 myotubes, followed by mass spectrometry (Figure 4A and Supplemental Figure 9). Two proteins were mutually identified from both techniques, NEB and LMOD3, which were validated for binding to KLHL40 by coimmunoprecipitation in nonmuscle COS7 cells (Figure 4B and refs. 33, 34).

NEB is a thin filament protein associated frequently with NM, but LMOD3 is a novel protein of unknown function (1). LMOD3 is highly homologous to LMOD2, an essential regulator of thin filament actin organization in cardiomyocytes, suggesting that both proteins share similar function (23). We found that LMOD3, like LMOD2, localized to the A band in both relaxed and contracted muscles (Figure 4, C and D). KLHL40 also localized to the A band (Figure 2B), suggesting that LMOD3 and KLHL40 colocalize. Interestingly, both LMOD2 and LMOD3 are specific to striated muscle. *Lmod2* was relatively more enriched in the heart compared with skeletal muscle while *Lmod3* was expressed at a higher level

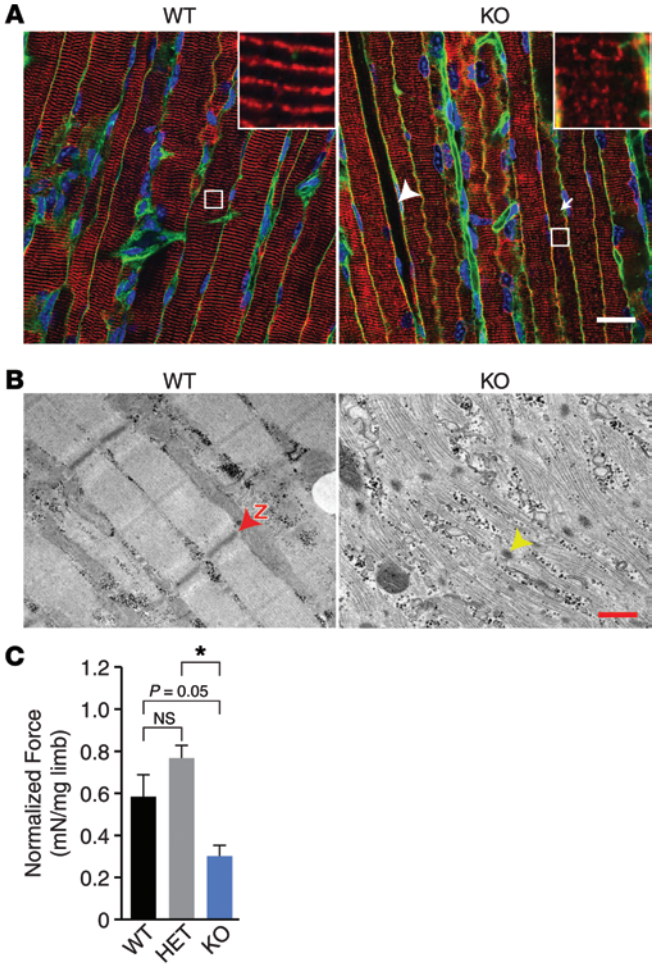

Figure 3. KO mice have disrupted muscle structure and function. (**A**) Longitudinal sections of P8 diaphragm muscles from WT and KO mice stained with desmin (red), DAPI (blue), and wheat germ agglutinin (green). The white arrow indicates disrupted myofibers. The white arrowhead denotes fibers staining abnormally for desmin that are more frequent in, but not specific to, KO muscles. Insets show normal striated pattern of Z lines in WT muscles but that some KO fibers have complete loss of sarcomere organization. Scale bar: 20 μm. (**B**) Electron microscopy analysis of longitudinal sections of P8 diaphragms from WT and KO mice shows some highly disorganized fibers. The red "Z" with red arrowhead indicates representative Z line in WT section. The yellow arrowhead denotes representative nemaline-like body. Scale bar: 1 μm. (**C**) Maximum contractile force of P1 WT, *Klhl40*$^{+/-}$ (HET), and KO hind limb following 150-Hz stimulation, normalized to limb mass. KO muscle shows greater than 50% loss of force compared with that of both WT and HET mice (WT, n = 6; HET, n = 17; and KO, n = 8). *P < 0.05, FDR = 0.05. Data are presented as mean ± SEM.

in skeletal muscle compared with heart, which agrees with previous studies on the expression of these proteins (Supplemental Figure 10 and ref. 24). The expression and localization data suggest that LMOD3 could function similarly to LMOD2, but perhaps specifically for skeletal muscle.

KLHL40 blocks proteasome-mediated LMOD3 degradation by inhibiting ubiquitination. KLHL40 belongs to the BBK protein family; its members serve as substrate-specific adaptors that mediate ubiquitination and degradation of their respective substrates (17–22). To determine whether KLHL40 mediates degradation of NEB and LMOD3, we coexpressed a fragment of NEB, NEB$_{frag}$, and LMOD3 with KLHL40 in COS7 cells. Unlike other BBK proteins, we found that KLHL40 dramatically increased protein levels of both NEB$_{frag}$ and LMOD3, without a corresponding change in respective mRNA transcripts (Figure 5 and Supplemental Figure 11). Addition of proteasome inhibitor was sufficient to increase LMOD3 levels comparably to KLHL40, again without a corresponding change in transcription (Supplemental Figure 11 and Supplemental Figure 12A). Proteasome inhibitor did not substantially increase NEB$_{frag}$ levels. Finally, we found that KLHL40 decreased K48 polyubiquitination of LMOD3, which specifically marks a protein for proteasome-mediated degradation (Supplemental Figure 12B and ref. 35). These data suggest that KLHL40 serves to increase NEB and LMOD3 levels and prevents degradation of LMOD3 by the proteasome.

Mapping the domains of KLHL40 that regulate LMOD3 and NEB. KLHL40 contains 3 annotated domains: BTB/POZ, BACK, and KR domains (Supplemental Figure 13A). To determine which domains are important for regulation of LMOD3 and NEB$_{frag}$, we generated various KLHL40 mutants lacking combinations of all annotated KLHL40 domains and coexpressed them with LMOD3-myc or NEB$_{frag}$-myc (Supplemental Figure 13B). Deletion of the KR domain abolished the stabilizing effect of KLHL40 on both LMOD3 and NEB$_{frag}$ levels. On the other hand, deletion of the BTB and/or BACK domains selectively diminished the stabilization of NEB$_{frag}$. These data suggest that the KLHL40 KR domain plays an essential role in KLHL40-mediated stabilization of both LMOD3 and NEB$_{frag}$, while the KLHL40 BTB and BACK domains are only essential for NEB$_{frag}$. None of these effects were due to changes in *Neb*$_{frag}$ or *Lmod3* transcription (Supplemental Figure 13C).

Loss of KLHL40 results in decreased NEB and LMOD3 in mice. We analyzed protein expression in skeletal muscles from P1 and P8 mice of different *Klhl40* genotypes and found that NEB was decreased by approximately 50%, while LMOD3 was nearly eliminated in KO mice (Figure 6, A and B, and Supplemental Figure 14, A–C). Notably, *Klhl40*$^{+/-}$ (HET) mice also had reduced LMOD3 compared with KLHL40 WT mice, without growth defects or early lethality (Figure 6B). Loss of NEB has been shown to result in shorter thin filament lengths, but KO mice did not have shortened thin filaments like *Neb*$^{-/-}$ mice (Supplemental Figure 15 and refs. 36–38).

Using quantitative mass spectrometry, we found that NEB and LMOD3 were among the most decreased proteins, with LMOD3 being the most downregulated in the entire muscle proteome (Fig-

Table 1. KLHL40 binding partners identified by yeast 2-hybrid analysis using a skeletal muscle cDNA library

Protein	Description	Positive clones[A]
LMOD3[B]	Putative actin nucleating factor	5
VDAC1	Mitochondrial voltage dependent anion channel	5
NEB[B]	Sarcomere protein	1
CC2D1B	Putative transcriptional repressor	1
AHNAK	Giant scaffold protein	1

[A]"Positive clones" indicates the number of yeast colonies surviving selection that encode for the indicated protein. [B]Protein binding partners mutually identified in TAP (Figure 4A) and by yeast 2-hybrid analysis.

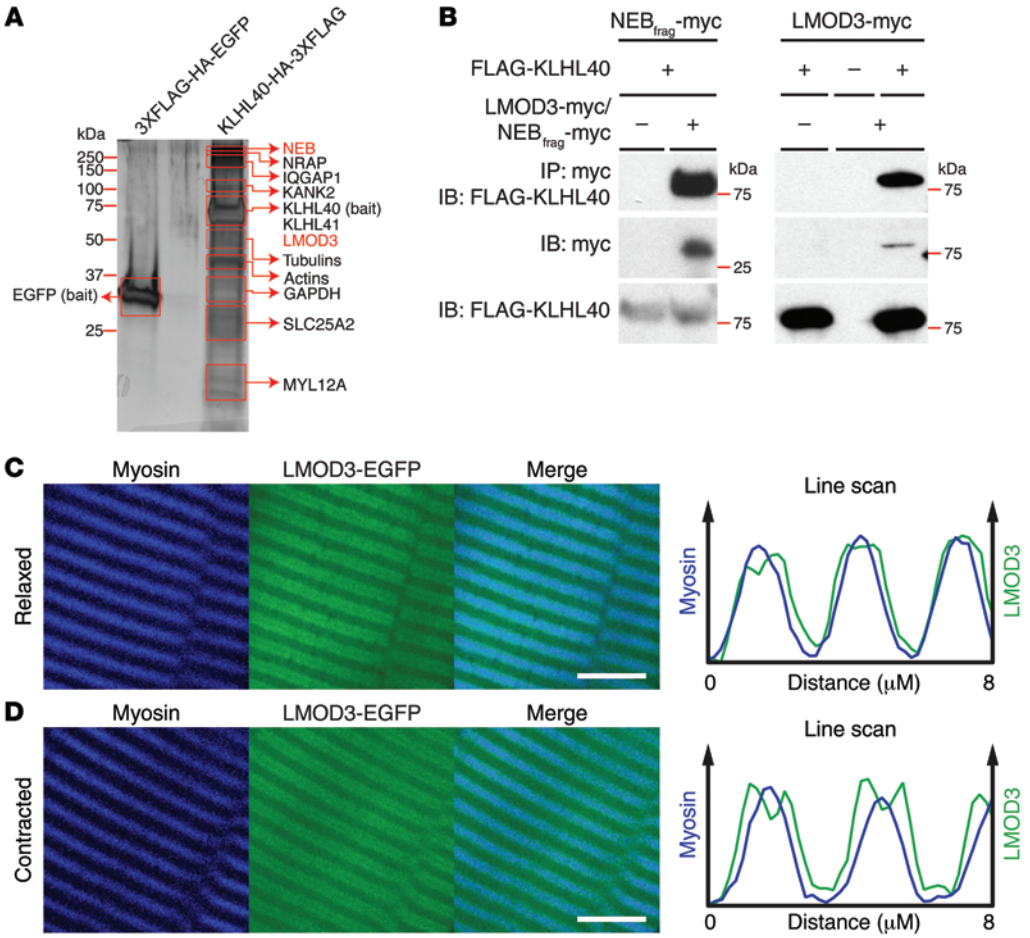

Figure 4. KLHL40 binds 2 thin filament proteins, NEB and LMOD3, and LMOD3 localizes to the sarcomere A band. (**A**) Top KLHL40 binding partners identified following TAP of KLHL40 from cultured C2C12 myotubes. A representative silver-stained gel with TAP protein from myotubes infected with 3XFLAG-HA-EGFP (negative control) or KLHL40-HA-3XFLAG is shown. Proteins listed next to each box indicate the most abundant protein(s) of the correct molecular weight identified in each corresponding area. Abundance is based on estimated enrichment using exponentially modified protein abundance index. TAP of 3XFLAG-HA-KLHL40 protein was also analyzed, and the same top-binding partners were identified (Supplemental Figure 9). Proteins shown in red (NEB and LMOD3) indicate KLHL40 binding partners mutually identified in the TAP and yeast 2-hybrid experiment (Table 1). (**B**) Coimmunoprecipitation of FLAG-KLHL40 with LMOD3-myc and NEB_{frag}-myc from COS7 cells. "–" refers to empty FLAG vector for FLAG-KLHL40 and empty myc vector for either LMOD3-myc or NEB_{frag}-myc. (**C** and **D**) LMOD3-EGFP localization relative to myosin in (**C**) relaxed muscles and (**D**) contracted muscles shows that LMOD3 resides in the sarcomere A band. Graphs are representative line scans of indicated signals calculated over 8 μm of distance along the length of the myofiber. Scale bar: 5 μm.

ure 6C). Of all proteins downregulated by greater than 1.5-fold, only LMOD3 and NEB were found to be binding partners by either of our nonbiased KLHL40 binding assays (Supplemental Table 2). Notably, no decrease was seen in *Neb* or *Lmod3* mRNA transcripts (Supplemental Figure 14, D–G).

Some patients with severe NM and KLHL40 deficiency have decreased LMOD3 and NEB. We analyzed LMOD3 and NEB in 3 different patients with 3 different sets of mutations in the *KLHL40* locus (Figure 7A). Patient 1 was a compound heterozygote for 2 missense mutations: R311L and T506P. Patient 2 was homozygous for a W90* nonsense mutation, while patient 3 was homozygous for an E528K missense mutation. Patients with the same mutation as patient 3 have a less clinically severe outcome than that observed with patients with other mutations of KLHL40 (12). Accordingly, the skeletal muscle biopsies showed that muscle pathology was more severe in patients 1 and 2 than in patient 3 (Supplemental Figure 16). Patients 1, 2, and 3 all had profoundly reduced KLHL40; however, patient 3 showed residual KLHL40. LMOD3 and NEB were reduced dramatically in patients 1 and 2, while LMOD3 protein remained relatively unchanged in patient 3 when compared with age-appropriate controls (control 1 for patients 1 and 2, and control 2 for patient 3) (Figure 7, B and C). NEB reduction in patient 3 was inconclusive due to issues with GAPDH signal for patient 3 and control 2. Given that patient 3 had some residual KLHL40 and less severe muscle pathology, our findings in mice that KLHL40 serves to stabilize NEB and LMOD3 are largely consistent in KLHL40-deficient patients, although there may be some mechanistic differences based on the type of *KLHL40* mutation.

Discussion

KLHL40 mutations have been shown recently to cause NM in humans, but the underlying pathogenic mechanisms have not been defined. The results of this study demonstrate that KLHL40 is essential for the maintenance of sarcomere structure and muscle contractility. Loss of KLHL40 in mice leads to

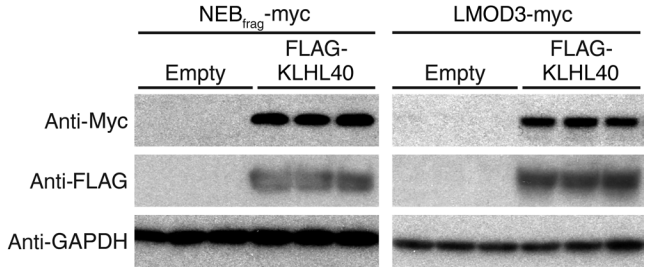

Figure 5. KLHL40 increases NEB$_{frag}$ and LMOD3 protein levels. Western blot analysis of COS7 cells expressing NEB$_{frag}$-myc or LMOD3-myc without (Empty) or with FLAG-KLHL40. GAPDH is used as a loading control.

a NM-like phenotype comparable to that of patients with NM lacking KLHL40 (12). We found that KLHL40 localizes to the I band and A band of sarcomeres and binds to 2 proteins located in these bands, NEB and LMOD3. Unlike previously described BBK proteins, we showed that KLHL40 promotes the stability of NEB and LMOD3, providing a possible molecular explanation for NM in KLHL40-deficient patients. Consistent with these findings, NEB and LMOD3 protein levels are specifically diminished in KLHL40-deficient mice and KLHL40-deficient patients, suggesting the involvement of KLHL40 in NM and regulation of sarcomere structure. We propose that KLHL40 regulates NEB and LMOD3 and that loss of KLHL40 primarily reduces NEB and LMOD3. This results in thin filament disruption, with subsequent irregularities of sarcomere Z-discs and, in extreme cases, sarcomere dissolution with the formation of ovoid Z-discs, culminating in a fatal loss of muscle function (Figure 8).

NM-like disease due to loss of Klhl40. Similar to human patients that lack KLHL40, KO mice display neonatal lethality, with defects in sarcomere structure and significant muscle weakness (12). Cardiac defects are not a typical feature of NM, and, although *Klhl40* has some expression in the heart, we did not observe cardiac hypertrophy, dilation, or any loss in cardiac contractility in KO mice (1, 39).

Unlike patient biopsies, classic nemaline bodies are not readily apparent in the KO mice, except in highly disorganized fibers in which they present as widened Z-discs. The more prevalent defect seen in mice is the presence of Z line streaming, which is indicative of sarcomere damage and is often seen in combination with nemaline bodies in patient biopsies (9, 40). The lack of bona fide nemaline bodies in other KO mouse models of NM is not uncommon. Deletion of *Acta1* and *Neb* in mice, the 2 most frequently implicated proteins in NM (1), results in neonatal lethality and muscle dysfunction, but classical nemaline bodies are not reported (36–38, 41). Currently, nemaline bodies are only reproduced in mouse models of NM in which mutant protein is overexpressed, suggesting that mutant proteins are required for protein aggregation to form rods (42–44). A previous study noted that the presence of nemaline bodies does not correlate with the severity of the disease (2). Instead, it is believed that decreased contractility due to primary defects in the sarcomere thin filament is the underlying cause for symptoms in NM (10). This hypothesis is supported by studies with P1 NEB-deficient mice, which have a dramatic loss in muscle contractility, with no visible sarcomere defects (36, 45). Accordingly, we too found that sarcomeres in P1 KLHL40 WT and KO mice appeared comparable, but there was still a greater than 50% loss of maximum tetanic force in KO muscle. Our data, combined with previous studies, corroborate the hypothesis that NM is likely due to sarcomere dysfunction and instability, causing a primary loss in muscle contractility (2, 36–38, 41). We believe that sarcomere instability results in the visible Z line streaming and nemaline bodies in KLHL40-deficient mice at later ages due to increased muscle use following birth.

KLHL40 binding and regulation of thin filament proteins, NEB and LMOD3. We have demonstrated that KLHL40 localizes to the sarcomere I band and the A band, which potentially explains the conflicting results from two previous reports showing I band and A band localization separately (12, 13). NEB is known to span the I band and the A band, and we have shown that LMOD3 occupies the A band (46). Thus, KLHL40 occupies the same subcellular compartments as NEB and LMOD3.

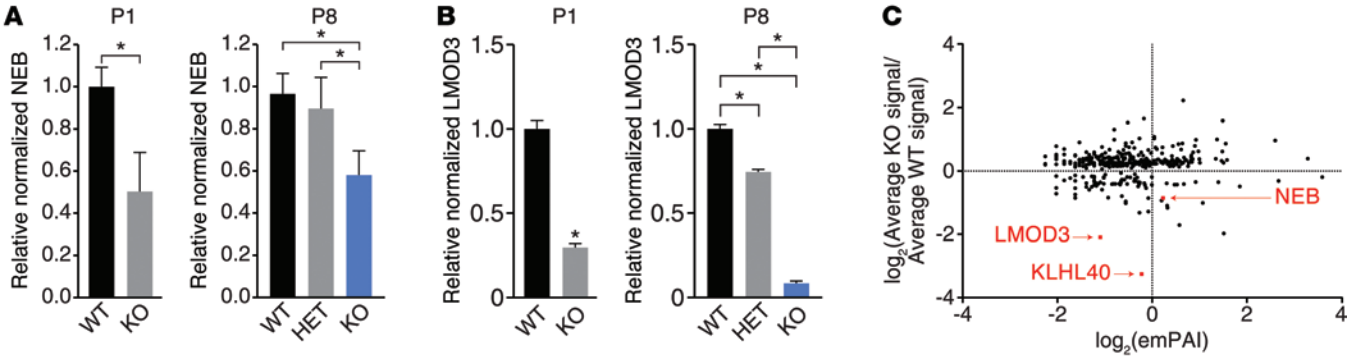

Figure 6. Reduced NEB and LMOD3 in KLHL40-deficient muscles. (**A** and **B**) Densitometry analysis of P1 and P8 quadriceps muscle (**A**) NEB dot blot and (**B**) LMOD3 Western blot shows downregulation of both proteins in KO muscles compared with WT muscles (see Supplemental Figure 14) (P1: WT and KO, $n = 3$; P8: WT, $n = 5$, HET, $n = 4$, and KO, $n = 5$). *$P < 0.05$, FDR = 0.05. Data are presented as mean ± SEM. (**C**) Quantitative proteomic analysis of relative protein changes between P6 WT ($n = 3$) and KO ($n = 3$) whole skeletal muscle shows that LMOD3 and NEB are 2 of the most downregulated proteins without corresponding changes in transcription (Supplemental Figure 14G). Data are arbitrarily stratified by exponentially modified protein abundance index (emPAI) to allow for better resolution of individual data points. Only proteins with significant ($P < 0.05$) changes between WT and KO mice are shown. Values for each point are listed in Supplemental Table 2.

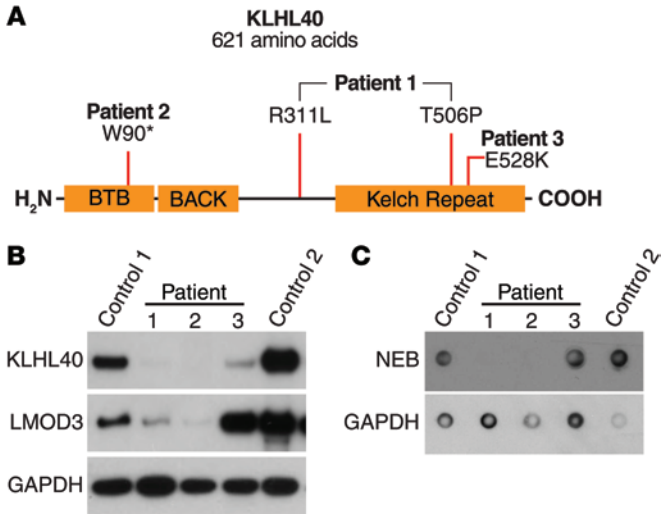

Figure 7. Analyzing LMOD3 and NEB expression in KLHL40-deficient patients. (**A**) Relative location of KLHL40 mutations in patients analyzed in **B** and **C**. Note that patient 1 is a compound heterozygote for the indicated mutations. (**B**) Detection of LMOD3 and KLHL40 by Western blot analysis and (**C**) NEB by dot blot analysis in control and KLHL40-deficient patient skeletal muscle biopsies. Patients 1 and 2 have a clear decrease in LMOD3 and NEB compared with age-matched control, control 1. Patient 3 compared with age-matched control, control 2, does not have decreased LMOD3, and changes in NEB are inconclusive due to issues with GAPDH signal. Control 1 and control 2 are 11-day-old and 6-month-old neonate controls, respectively. Patient 1 was biopsied at 2 days, patient 2 was biopsied at 25 days, and patient 3 was biopsied at 3 months of age. GAPDH is shown for loading control.

In contrast to all other described BBK proteins, we have demonstrated that KLHL40 actually stabilizes, rather than degrades, its substrates (15–22). NEB_{frag} and LMOD3 are increased in cell culture with KLHL40 expression, and loss of KLHL40 in mice results in reduced NEB and LMOD3 independent of any transcriptional changes. In addition, KLHL40 appears to block LMOD3 ubiquitination, whereas KLHL40 regulates NEB_{frag} in a proteasome-independent manner. These findings provide the first example of a BBK protein that can mediate protein stabilization rather than degradation.

Previous studies showed that the KR domain in BBK proteins is required for binding of substrate to its respective BBK protein (20–22). Accordingly, deletion of the KLHL40 KR domain abrogates stabilization of LMOD3 and NEB_{frag} in cell culture. Deletion of the BTB or BACK domains of KLHL40 has no effect on LMOD3 stabilization, but NEB_{frag} levels are reduced, again, implying alternative mechanisms for KLHL40 regulation of NEB_{frag}.

BBK proteins typically bind the CUL3-E3 ligase complex to mediate substrate recognition for ubiquitination (15–22). It is possible that KLHL40 prevents CUL3-mediated degradation of LMOD3, perhaps by preventing recognition of LMOD3 by the CUL3-E3 complex. Alternatively, based on KLHL40's differential localization in relaxed and contracted muscles, KLHL40 may have a more chaperone-like function to maintain proper LMOD3 and NEB folding throughout muscle contraction, which secondarily prevents their degradation. Further experiments are required to understand the role of KLHL40 during muscle contraction and to elucidate its unique pro-stability function. It will be of interest to determine whether other BBK proteins also stabilize their substrates.

Role of decreased NEB and LMOD3 in NM phenotype. Whole-proteome analysis of KO muscle revealed that NEB and LMOD3 were among the most downregulated proteins and were the only identified binding partners to show such dramatic regulation. LMOD3 was the most reduced protein in the entire muscle proteome. In fact, even 50% reduction of *Klhl40* transcript in mice lacking a single copy of the *Klhl40* gene was sufficient to reduce LMOD3, suggesting a tight dose dependence of LMOD3 on KLHL40 protein levels.

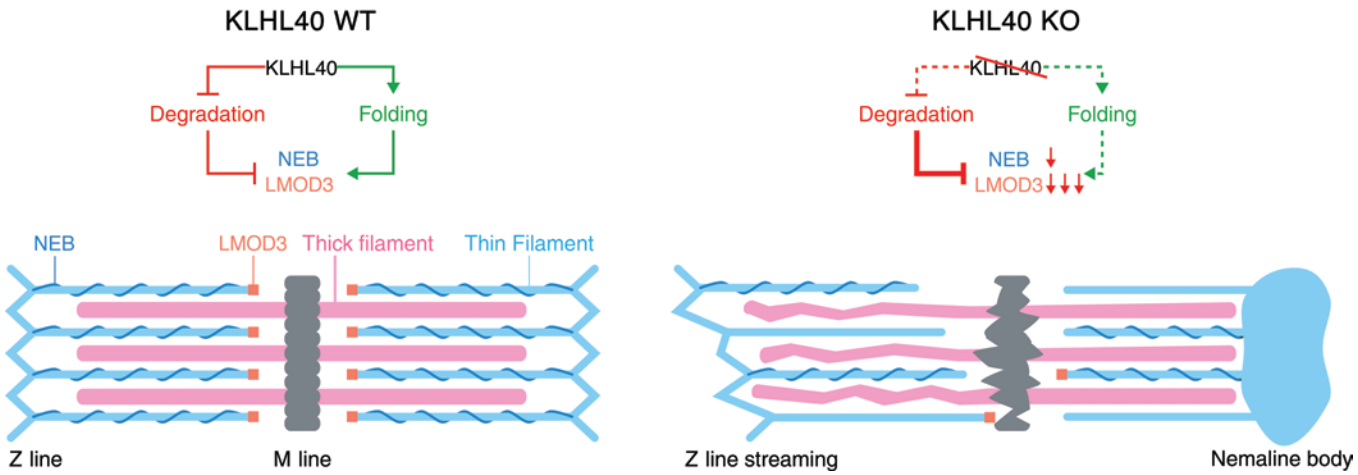

Figure 8. Proposed mechanism of NM pathogenesis due to loss of KLHL40. Under normal conditions, KLHL40 either blocks the degradation or promotes successful folding of NEB and LMOD3, which function to stabilize the thin filament, allowing normal sarcomere function. In muscles lacking KLHL40, NEB and LMOD3 protein levels are reduced, resulting in destabilization of thin filaments, sarcomere dysfunction, and subsequent NM.

Previous work has shown definitively that mutations in *NEB* in patients and loss of *Neb* in mice results in NM, suggesting that decreased NEB in KO mice could contribute to the NM phenotype (1, 4, 36–38). A pervading belief is that NEB acts as a molecular ruler to regulate thin filament lengths based on shortened thin filament lengths seen in *Neb*-deficient mice (36, 37, 47). However, more recent studies argue that NEB deficiency contributes directly to a loss in muscle contractility due to dysregulation of actin-myosin crossbridge formation (45, 47, 48). Accordingly, we see over a 50% loss in hind limb strength of P1 KO mice, which have approximately 50% reduction in NEB, without any evidence of sarcomere defects. It is possible that KLHL40 loss functionally impairs the actin-myosin crossbridge activity of NEB.

LMOD3 function has hitherto not been defined, and it has not yet been implicated in any disease. Our study presents the first evidence of a possible role of LMOD3 in NM. LMOD3 is highly homologous to LMOD2, which was shown previously to be vital for sarcomere structure in cardiomyocytes by regulating actin assembly at the pointed end of thin filaments (near the sarcomere M line) (23). Indeed, we found that LMOD3 localizes to the A band in a matter similar to that of LMOD2, likely indicating that LMOD3 also binds the pointed end of actin filaments. Thus, loss of LMOD3, secondary to KLHL40 deficiency, may lead to thin filament actin dysregulation.

Role of BBK proteins in human NM. Thus far, 3 BBK proteins have been implicated in NM: KBTBD13, KLHL40, and KLHL41 (11–13). Our study is the first to define a possible molecular mechanism for any of these proteins. Consistent with the phenotype of KLHL40 mutant mice, the 2 patients with NM (patients 1 and 2) completely deficient for KLHL40 had marked reduction in LMOD3 and NEB, while a third patient (patient 3), with some residual KLHL40, had relatively normal LMOD3. Patients with the same mutation as patient 3 present with less severe clinical symptoms compared with patients with all other KLHL40 mutations (12). Thus, our finding that KLHL40 serves to stabilize LMOD3 in mice is largely consistent in KLHL40-deficient patients, although there may be some mechanistic differences based on the type of KLHL40 mutation. Regardless, these findings may have important therapeutic implications for KLHL40-deficient patients (see below).

A recent report described *KLHL41* mutations causing NM in humans (13). KLHL41 is the most closely related protein to KLHL40 (71% by BLASTP alignment) (13, 49–51). Interestingly, we found that KLHL41 was the most enriched KLHL40 binding partner from C2C12 myotubes. As determined by quantitative proteomics, KLHL41 levels in KLHL40-deficient mice were not changed, suggesting that KLHL40 does not regulate protein levels of KLHL41. We hypothesize that KLHL40 and KLHL41 may form a heterodimer or polymer to regulate thin filament proteins with both KLHL40 and KLHL41 performing unique, nonredundant functions, possibly explaining why a disruption in either protein results in NM. It is also tempting to speculate that KLHL41, like KLHL40, promotes the stability of its substrates based on their close homology. On the other hand, KBTBD13 is much more distantly related to KLHL40 and KLHL41, and *KBTBD13* mutations resulting in NM are autosomal dominant in contrast to the autosomal recessive transmission of *KLHL40*- and *KLHL41*-related NM (51). Thus, the molecular mechanism underlying KBTBD13 NM is likely different than that of KLHL40 and KLHL41.

Therapeutic implications. There are currently no therapies available to treat NM. However, our data suggest that KLHL40 deficiency results in NM by secondary loss of NEB and LMOD3 protein and that proteasome inhibition may be sufficient to restore LMOD3. Should LMOD3 be determined to be a major contributor to the NM phenotype seen with KLHL40 deficiency, it would be worthwhile to explore whether proteasome inhibition can alleviate muscle dysfunction in KLHL40-deficient patients. Proteasome inhibitors have already been used in cancer therapy and are thus available for clinical use (52). Therefore, further delineation of the molecular mechanism by which KLHL40 promotes NEB and LMOD3 stability may allow for the development of the first therapy for NM.

Methods

Generation of Klhl40$^{+/-}$, KO, and MCK-Klhl40 mice. *Klhl40*-deficient mice were generated using a targeted *Klhl40* embryonic stem cell clone (#14780A-B6) obtained from the KOMP Repository (http://www.KOMP.org) (27), as described previously (53). *Klhl40$^{+/-}$* mice were intercrossed to generate KO mice and maintained in a pure C57BL/6 background.

MCK-Klhl40 transgenic mice were generated as previously described by placing the murine *Klhl40* cDNA under the control of a 4.8-kb fragment of the MCK promoter and deriving transgenic mice on a B6C3F1 background (28, 54, 55). *MCK-Klhl40* mice were intercrossed to C57BL/6 *Klhl40$^{+/-}$* mice to generate a mixed background. All analyses were done within the same mixed line using littermates as controls. Genotyping primers are available in the Supplemental Methods.

Protein localization by electroporation of flexor digitorum brevis muscles and second harmonic generation. KLHL40-EGFP, LMOD3-EGFP, ACTN1A-EGFP, and TMOD4-EGFP were localized to myosin by second harmonic generation, as previously described, with some modifications (30, 56). Skinned feet from mice were immersed in either an ice-cold, calcium-free EDTA-Ringer's solution (100 mM NaCl, 2 mM KCl, 2 mM $MgCl_2$, 6 mM KH_2PO_4, 1 mM EDTA, and 0.1% glucose) or in an ice-cold rigor buffer (100 mM KCl, 2 mM $MgCl_2$, 1 mM EDTA, and 10 mM KH_2PO_4) (31). Feet were left in buffer for at least 2 hours and then imaged, as described previously (56). Line scan analyses were done using Fiji ImageJ software (57).

Neonatal muscle contraction. After euthanasia, hind limbs of P1 pups were placed in an incubated 30°C oxygenated (95% O_2, 5% CO_2) physiological salt solution (58). The foot was placed in a clamp at the base of the bath, and the femur was tied with 6-O suture from just above the knee to the arm of a dual-mode servomotor (300B, Aurora Scientific Inc.). Resting tension was maintained by a stepper motor. Contractile data were obtained at a resting tension of 0.5 g (i.e., optimal length), with electrical stimulation at 30 V and a 500 μs pulse width. Data were obtained and analyzed with Dynamic Muscle Control (DMC v.4.1.6) and Dynamic Muscle Analysis (DMA v.3.2) software, respectively (Aurora Scientific Inc.). Following initial twitch and tetanic contractions, a force-frequency relationship was determined over the range 1–150 Hz. Normalized force was expressed as mN/mg limb mass.

RNA expression. RNA levels were measured by in situ hybridization, Northern blot, and qPCR, as previously described (53, 59). The

methods are described in detail and primers are provided in the Supplemental Materials.

Microarray analysis. RNA was submitted to the UT Southwestern Genomic and Microarray Core Facility for further processing and microarray analysis using a MouseWG-6 V2 BeadChip (Illumina), as previously described (60). Significant ($P < 0.05$) changes in sarcomere genes are reported in Supplemental Table 1. Data are available from Gene Expression Omnibus (accession no. GSE56570).

Histology, immunochemistry, and X-gal staining. Skeletal muscle tissues were fixed in 4% paraformaldehyde and processed for paraffin histology, as previously described (53). Imaging was done by confocal microscopy using a Zeiss LSM 710 microscope. X-gal staining is described in the Supplemental Methods.

Electron microscopy. Processing of muscle tissues for electron microscopy was performed as previously described (61). Images were acquired using a FEI Tecnai G2 Spirit Biotwin transmission electron microscope.

Muscle yeast 2-hybrid screen. KLHL40 yeast 2-hybrid analysis was performed using the Clontech Matchmaker Gold Yeast Two-Hybrid System with a Mate & Plate — Human Skeletal Muscle cDNA library according to the manufacturer's recommended instructions.

Cloning of epitope-tagged constructs for electroporation, protein stability, and immunoprecipitation experiments. Details regarding cloning are provided in the Supplemental Methods.

TAP of KLHL40 from C2C12 cells and protein identification. Details regarding the KLHL40 TAP experiment can be found in the Supplemental Methods.

KLHL40 binding and stabilization of NEB_{frag} and LMOD3 in COS7 cells. FLAG-KLHL40 and NEB_{frag}-myc or LMOD3-myc were cotransfected into COS7 cells. Protein was extracted, and coimmunoprecipitation of NEB_{frag}-myc or LMOD3-myc with FLAG-KLHL40 was performed. For stability experiments, NEB_{frag}-myc and LMOD3-myc levels were analyzed by standard Western blotting. Details regarding KLHL40 coimmunoprecipitation with NEB_{frag} and LMOD3 and protein stability experiments can be found in the Supplemental Methods.

Ubiquitination analysis of LMOD3 in COS7 cells. COS7 cells were transfected with LMOD3-myc and FLAG-KLHL40, as stated above. Protein was collected in denaturing lysis buffer (see Supplemental Methods). Ubiquitinated protein was immunoprecipitated with K48 anti-ubiquitin antibody (Apu2, EMD Millipore), and ubiquitinated LMOD3-myc levels were visualized by standard Western blotting. See Supplemental Methods for additional details.

Immunoblotting LMOD3 and GAPDH in skeletal muscle. For LMOD3 and GAPDH, a standard immunoblot was performed using protein extracted from neonatal quadriceps muscles (see Supplemental Methods for protocol) with anti-LMOD3 (14948-1-AP, Proteintech) and anti-GAPDH (MAB374, EMD Millipore) primary antibodies, followed by appropriate HRP-conjugated secondary antibodies (Bio-Rad). See the Supplemental Methods for additional details.

Dot blot analysis of NEB and GAPDH in skeletal muscle. Quadriceps muscle protein was loaded onto a nitrocellulose membrane (Bio-Rad) using a Bio-Dot microfiltration apparatus (Bio-Rad) according to the manufacturer's instructions. The blot was subsequently processed like a standard immunoblot, with NEB and GAPDH analyzed on 2 separate blots. NEB was analyzed with an anti-NEB antibody (19706-1-AP, Proteintech), and GAPDH was analyzed using anti-GAPDH antibody (MAB374, EMD Millipore). Following primary antibodies, the appropriate HRP-conjugated secondary antibody was used. Additional details regarding the dot blot protocol can be found in the Supplemental Methods.

Quantitative proteomic analysis of skeletal muscle. Protein from quadriceps of P6 mice (3 WT and 3 KO mice) was extracted and processed as outlined in the corresponding Supplemental Methods section. Each of the samples was labeled with a separate isobaric label using the TMT Mass Tagging Kit (TMTsixplex, Thermo Scientific), combined into a single sample, concentrated, and loaded into a 2D LC-MS. Analysis was done using Mascot software using the Proteome Sciences 6-plex Tandem Mass Tags quantitation method. Additional details can be found in the Supplemental Methods.

Analysis of muscle samples from KLHL40-deficient patients. Western blot analysis was performed on patient and healthy human control muscle biopsies, as previously described (12). Additional details regarding protein extraction and immunoblot materials can be found in the Supplemental Methods. Gomori trichrome staining of patient muscle sections was performed as described previously (62).

Statistics. Data are presented as mean ± SEM. Differences between 2 groups were tested for statistical significance using the unpaired 2-tailed Student's *t* test. $P < 0.05$ was considered significant. For analysis of multiple groups, we used the Holm-Sidak correction for multiple comparisons with a false discovery rate (FDR) of 0.05.

Study approval. All experimental procedures involving animals in this study were reviewed and approved by the University of Texas Southwestern Medical Center's Institutional Animal Care and Use Committee. All human subjects were enrolled following informed consent, and research was conducted according to protocols approved by the Human Research Ethics Committee of the University of Western Australia.

Acknowledgments

We are grateful to Xiaoxia Qi, John R. McAnally, and Xiang Chen for technical assistance. We thank Robyn Leidel, Karen Rothberg, Kate Luby-Phelps, and Christopher Gilpin for assistance and advice in the UT Southwestern Electron Microscopy Core Facility as well as John Shelton and James Richardson for help with histology and imaging. We thank Marie-Louise Bang (Istituto di Ricerca Genetica e Biomedica) for providing tissue from NEB-deficient mice. We thank Jose Cabrerra for assistance with graphics. This work was supported by grants from the NIH (HL-077439, HL-111665, HL-093039, DK-099653, and U01-HL-100401) and the Robert A. Welch Foundation (grant 1-0025 to E.N. Olson). A. Garg is supported by a T32 NIH training grant (T32-HL-007360). G. Ravenscroft and N.G. Laing are supported by Australian National Health and Medical Research Council (NHMRC) Early Career and Principal Research Fellowships APP1035955 and APP1022707 and NHMRC project grant APP1022707.

Address correspondence to: Eric N. Olson, Department of Molecular Biology, 5323 Harry Hines Blvd., Dallas, Texas 75390-9148, USA. Phone: 214.648.1187; Fax: 214.648.1196; E-mail: eric.olson@utsouthwestern.edu.

Jason O'Rourke's present address is: Genomics Institute of the Novartis Research Foundation, San Diego, California, USA.

1. Wallgren-Pettersson C, Sewry CA, Nowak KJ, Laing NG. Nemaline myopathies. *Semin Pediatr Neurol*. 2011;18(4):230–238.
2. Shimomura C, Nonaka I. Nemaline myopathy: comparative muscle histochemistry in the severe neonatal, moderate congenital, and adult-onset forms. *Pediatr Neurol*. 1989;5(1):25–31.
3. Laing NG, et al. A mutation in the α tropomyosin gene TPM3 associated with autosomal dominant nemaline myopathy NEM1. *Nat Genet*. 1995;10(2):249.
4. Lehtokari VL, et al. Identification of 45 novel mutations in the nebulin gene associated with autosomal recessive nemaline myopathy. *Hum Mutat*. 2006;27(9):946–956.
5. Nowak KJ, et al. Mutations in the skeletal muscle α-actin gene in patients with actin myopathy and nemaline myopathy. *Nat Genet*. 1999;23(2):208–212.
6. Donner K, et al. Mutations in the β-tropomyosin (TPM2) gene — a rare cause of nemaline myopathy. *Neuromuscul Disord*. 2002;12(2):151–158.
7. Johnston JJ, et al. A novel nemaline myopathy in the Amish caused by a mutation in troponin T1. *Am J Hum Genet*. 2000;67(4):814–821.
8. Agrawal PB, et al. Nemaline myopathy with minicores caused by mutation of the CFL2 gene encoding the skeletal muscle actin-binding protein, cofilin-2. *Am J Hum Genet*. 2007;80(1):162–167.
9. Franzini-Armstrong C, Lee Sweeney H. The contractile machinery of skeletal muscle. In: Hill JA, Olson EN, eds. *Muscle*. Boston, Massachusetts, USA: Academic Press; 2012:823–840.
10. Nance JR, Dowling JJ, Gibbs EM, Bönnemann CG. Congenital myopathies: an update. *Curr Neurol Neurosci Rep*. 2012;12(2):165–174.
11. Sambuughin N, et al. Dominant mutations in KBTBD13, a member of the BTB/Kelch family, cause nemaline myopathy with cores. *Am J Hum Genet*. 2010;87(6):842–847.
12. Ravenscroft G, et al. Mutations in KLHL40 are a frequent cause of severe autosomal-recessive nemaline myopathy. *Am J Hum Genet*. 2013;93(1):6–18.
13. Gupta VA, et al. Identification of KLHL41 mutations implicates BTB-Kelch-mediated ubiquitination as an alternate pathway to myofibrillar disruption in nemaline myopathy. *Am J Hum Genet*. 2013;93(6):1108–1117.
14. Stogios PJ, Privé GG. The BACK domain in BTB-kelch proteins. *Trends Biochem Sci*. 2004;29(12):634–637.
15. Bennett EJ, Rush J, Gygi SP, Harper JW. Dynamics of cullin-RING ubiquitin ligase network revealed by systematic quantitative proteomics. *Cell*. 2010;143(6):951–965.
16. Emanuele MJ, et al. Global identification of modular cullin-RING ligase substrates. *Cell*. 2011;147(2):459–474.
17. Zhang DD, Lo SC, Sun Z, Habib GM, Lieberman MW, Hannink M. Ubiquitination of Keap1, a BTB-Kelch substrate adaptor protein for Cul3, targets Keap1 for degradation by a proteasome-independent pathway. *J Biol Chem*. 2005;280(34):30091–30099.
18. Angers S, et al. The KLHL12-Cullin-3 ubiquitin ligase negatively regulates the Wnt-β-catenin pathway by targeting Dishevelled for degradation. *Nat Cell Biol*. 2006;8(4):348–357.
19. Sumara I, et al. A Cul3-based E3 ligase removes Aurora B from mitotic chromosomes, regulating mitotic progression and completion of cytokinesis in human cells. *Dev Cell*. 2007;12(6):887–900.
20. Lee YR, Yuan WC, Ho HC, Chen CH, Shih HM, Chen RH. The Cullin 3 substrate adaptor KLHL20 mediates DAPK ubiquitination to control interferon responses. *EMBO J*. 2010;29(10):1748–1761.
21. Jin L, et al. Ubiquitin-dependent regulation of COPII coat size and function. *Nature*. 2012;482(7386):495–500.
22. Shibata S, Zhang J, Puthumana J, Stone KL, Lifton RP. Kelch-like 3 and Cullin 3 regulate electrolyte homeostasis via ubiquitination and degradation of WNK4. *Proc Natl Acad Sci U S A*. 2013;110(19):7838–7843.
23. Chereau D, et al. Leiomodin is an actin filament nucleator in muscle cells. *Science*. 2008;320(5873):239–243.
24. Nanda V, Miano JM. Leiomodin 1, a new serum response factor-dependent target gene expressed preferentially in differentiated smooth muscle cells. *J Biol Chem*. 2012;287(4):2459–2467.
25. Gray PA, et al. Mouse brain organization revealed through direct genome-scale TF expression analysis. *Science*. 2004;306(5705):2255–2257.
26. Liu N, et al. Requirement of MEF2A, C, D for skeletal muscle regeneration. *Proc Natl Acad Sci U S A*. 2014;111(11):4109–4114.
27. Valenzuela DM, et al. High-throughput engineering of the mouse genome coupled with high-resolution expression analysis. *Nat Biotechnol*. 2003;21(6):652–659.
28. Sternberg EA, Spizz G, Perry WM, Vizard D, Weil T, Olson EN. Identification of upstream and intragenic regulatory elements that confer cell-type-restricted and differentiation-specific expression on the muscle creatine kinase gene. *Mol Cell Biol*. 1988;8(7):2896–2909.
29. Johnson JE, Wold BJ, Hauschka SD. Muscle creatine kinase sequence elements regulating skeletal and cardiac muscle expression in transgenic mice. *Mol Cell Biol*. 1989;9(8):3393–3399.
30. DiFranco M, Quinonez M, Capote J, Vergara J. DNA transfection of mammalian skeletal muscles using in vivo electroporation. *J Vis Exp*. 2009;pii(32):1520.
31. Knight PJ, Trinick JA. Preparation of myofibrils. *Methods Enzymol*. 1982;85(pt B):9–12.
32. Gokhin DS, Kim NE, Lewis SA, Hoenecke HR, D'Lima DD, Fowler VM. Thin-filament length correlates with fiber type in human skeletal muscle. *Am J Physiol Cell Physiol*. 2012;302(3):C555–C565.
33. Jensen FC, Girardi AJ, Gilden RV, Koprowski H. Infection of human and simian tissue cultures with Rous sarcoma virus. *Proc Natl Acad Sci U S A*. 1964;52:53–59.
34. Gluzman Y. SV40-transformed simian cells support the replication of early SV40 mutants. *Cell*. 1981;23(1):175–182.
35. Johnson ES. Ubiquitin branches out. *Nat Cell Biol*. 2002;4(12):E295–E298.
36. Bang ML, et al. Nebulin-deficient mice exhibit shorter thin filament lengths and reduced contractile function in skeletal muscle. *J Cell Biol*. 2006;173(6):905–916.
37. Witt CC, et al. Nebulin regulates thin filament length, contractility, and Z-disk structure in vivo. *EMBO J*. 2006;25(16):3843–3855.
38. Gokhin DS, Bang ML, Zhang J, Chen J, Lieber RL. Reduced thin filament length in nebulin-knockout skeletal muscle alters isometric contractile properties. *Am J Physiol Cell Physiol*. 2009;296(5):C1123–C1132.
39. Hill JA, Olson EN. Cardiac plasticity. *N Engl J Med*. 2008;358(13):1370–1380.
40. Agrawal PB, et al. Heterogeneity of nemaline myopathy cases with skeletal muscle α-actin gene mutations. *Ann Neurol*. 2004;56(1):86–96.
41. Crawford K, et al. Mice lacking skeletal muscle actin show reduced muscle strength and growth deficits and die during the neonatal period. *Mol Cell Biol*. 2002;22(16):5887–5896.
42. Corbett MA, et al. A mutation in α-tropomyosin(slow) affects muscle strength, maturation and hypertrophy in a mouse model for nemaline myopathy. *Hum Mol Genet*. 2001;10(4):317–328.
43. Ravenscroft G, et al. Mouse models of dominant ACTA1 disease recapitulate human disease and provide insight into therapies. *Brain*. 2011;134(pt 4):1101–1115.
44. Nowak KJ, et al. Nemaline myopathy caused by absence of alpha-skeletal muscle actin. *Ann Neurol*. 2007;61(2):175–184.
45. Bang ML, et al. Nebulin plays a direct role in promoting strong actin-myosin interactions. *FASEB J*. 2009;23(12):4117–4125.
46. Pappas CT, Bliss KT, Zieseniss A, Gregorio CC. The Nebulin family: an actin support group. *Trends Cell Biol*. 2011;21(1):29–37.
47. Ottenheijm CA, et al. Deleting exon 55 from the nebulin gene induces severe muscle weakness in a mouse model for nemaline myopathy. *Brain*. 2013;136(pt 6):1718–1731.
48. Chandra M, et al. Nebulin alters cross-bridge cycling kinetics and increases thin filament activation: a novel mechanism for increasing tension and reducing tension cost. *J Biol Chem*. 2009;284(45):30889–30896.
49. Altschul SF, et al. Gapped BLAST and PSI-BLAST: a new generation of protein database search programs. *Nucleic Acids Res*. 1997;25(17):3389–3402.
50. Altschul SF, et al. Protein database searches using compositionally adjusted substitution matrices. *FEBS J*. 2005;272(20):5101–5109.
51. Canning P, et al. Structural basis for Cul3 protein assembly with the BTB-Kelch family of E3 ubiquitin ligases. *J Biol Chem*. 2013;288(11):7803–7814.
52. Rastogi N, Mishra DP. Therapeutic targeting of cancer cell cycle using proteasome inhibitors. *Cell Div*. 2012;7(1):26.
53. Millay DP, et al. Myomaker is a membrane activator of myoblast fusion and muscle formation. *Nature*. 2013;499(7458):301–305.
54. Kim MS, et al. Protein kinase D1 stimulates MEF2 activity in skeletal muscle and enhances muscle performance. *Mol Cell Biol*. 2008;28(11):3600–3609.
55. Naya FJ, Mercer B, Shelton J, Richardson JA,

Williams RS, Olson EN. Stimulation of slow skeletal muscle fiber gene expression by calcineurin in vivo. *J Biol Chem*. 2000; 275(7):4545–4548.
56. Nelson BR, et al. Skeletal muscle-specific T-tubule protein STAC3 mediates voltage-induced Ca2+ release and contractility. *Proc Natl Acad Sci U S A*. 2013;110(29):11881–11886.
57. Schindelin J, et al. Fiji: an open-source platform for biological-image analysis. *Nat Methods*. 2012;9(7):676–682.
58. Wolff AV, et al. Passive mechanical properties of maturing extensor digitorum longus are not affected by lack of dystrophin. *Muscle Nerve*. 2006;34(3):304–312.
59. Shelton JM, Lee MH, Richardson JA, Patel SB. Microsomal triglyceride transfer protein expression during mouse development. *J Lipid Res*. 2000;41(4):532–537.
60. Aurora AB, et al. Macrophages are required for neonatal heart regeneration. *J Clin Invest*. 2014;124(3):1382–1392.
61. Li S, et al. Requirement for serum response factor for skeletal muscle growth and maturation revealed by tissue-specific gene deletion in mice. *Proc Natl Acad Sci U S A*. 2005;102(4):1082–1087.
62. Dubowitz V, Sewry CA. *Muscle Biopsy — A Practical Approach*. Philadelphia, Pennsylvania, USA: Elsevier Limited; 2007.